Preparation and Supramolecular Self-Assembly of a Polypeptide-*block*-polypseudorotaxane

Hsin-Fang Lee,[†] Hwo-Shuenn Sheu,[‡] U-Ser Jeng,[‡] Chih-Feng Huang,[†] and Feng-Chih Chang*,[†]

Institute of Applied Chemistry, National Chiao-Tung University, Hsin-Chu, Taiwan, and National Synchrotron Radiation Research Center, Hsinchu Science Park, Taiwan

Received February 4, 2005; Revised Manuscript Received May 30, 2005

ABSTRACT: We have successfully prepared a new class of self-assembled biomaterial: a polypeptide-*block*-polypseudorotaxane diblock copolymer. This diblock copolymer is comprised of an α-helical polypeptide rod, based on γ-benzyl-L-glutamate, and an originally coiled segment P(EO_{19}-*r*-PO_3); it forms inclusion complexes with α-cyclodextrins (α-CDs) to give crystalline polypseudorotaxanes. Formation of the polypseudorotaxane converts the conformation of P(EO_{19}-*r*-PO_3) from a flexible chain into a rodlike structure, which results in a novel block copolymer exhibiting a rod−rod conformation. Intrinsic interactions (e.g., the polypseudorotaxane's channel-type crystallization, the polypeptide's secondary structure, and microphase separation) within and between these rod−rod diblock copolymers contribute to their hierarchical self-assembly behavior, which we characterized using DSC, ^{1}H NMR spectroscopy, ^{13}C CP/MAS NMR spectroscopy, WAXS, and SAXS. The data obtained from the WAXS and SAXS studies clearly indicate the formation of juxtaposed bilayer-like nanostructure featuring hexagonally packed PBLG stacks and channel-type polypseudorotaxane moieties.

Introduction

One of the most fascinating subjects in nanochemistry and biomimetic chemistry is the creation of supramolecular architectures possessing well-defined shapes and functions. Self-assembly is the key in the design of many new functional supramolecular materials, and block copolymers are especially good candidates for producing self-assembled materials and nanometer-scale devices.[1,2] Two main types of block copolymers have been studied, namely the coil−coil and rod−coil copolymers. The latter type represents a special class of block copolymers that have attracted an increasing amount of attention during the past 5−10 years,[3,4] but, nevertheless, only a few publications have described the hierarchical self-assembly of rod−rod diblock copolymers.[5] Conventional polymer synthesis methods allow the preparation of a wide variety of materials for diverse applications, but the next generation of advanced materials will likely use design concepts borrowed from biological systems, such as tissue and bone, in which complex hierarchical structures are synthesized with very high specificity. These materials are characterized by multiple levels of structural organization, well-defined molecular architectures, and the presence of biological recognition sites.[6,7] By combining a knowledge of protein structure with fundamental concepts of polymer materials science, nonnatural protein-based materials can be designed that are capable of self-assembling into unique and uniform two- or three-dimensional topologies. Ultimately, it may become possible to design biopolymers capable of forming hierarchically ordered systems having multiple levels of interactive structure. Such materials have particular potential for biomedical use in drug delivery,[8] tissue regeneration,[9] environmentally responsive biomaterials, and other areas.[10]

Polypeptides are often used as precursor materials in biomedical applications because they can be synthesized to mimic natural proteins; i.e., they exhibit similar biocompatibility, degradation, and mechanical properties.[6−10] Synthetic polypeptide-based diblock copolymers usually exhibit the phase behavior of rod−coil block copolymers because their α-helical polypeptide units can act as rodlike mesogens.[11,12] When compared with most of the rod−coil type polymers that have been investigated so far, these peptide-based diblock copolymers possess a few unique features.[13−17] For example, the conformation of the polypeptide rod segment can be manipulated reversibly under the action of appropriate external stimuli; in addition, the self-assembly of these molecules is also driven by directed hydrogen-bonding interactions. Peptides of poly(γ-benzyl-L-glutamate) (PBLG) are typical helical polypeptides having a stiff rigid-rod structure that exhibits thermotropic and lyotropic liquid-crystalline properties. The peptides with degree of polymerization below 18 can exist both in the α-helical and in the β-sheet conformations, whereas for longer chains (degree of polymerization larger than 18), the intramolecular hydrogen bonds stabilized mainly the α-helical conformations.[18,19]

Polypseudorotaxanes are self-assembled supramacromolecules consisting of cyclic host materials and threaded guest molecules. Cyclodextrins, cucurbiturils, and porphyrins have been investigated extensively as host molecules for specific assembled structures. A large number of reports have been published on the formation of polypseudorotaxanes, i.e., inclusion complexes possessing channel-type supramolecular structures between cyclodextrins and various homopolymers or block copolymers.[20−25] In particular, inclusion complexes of poly(ethylene glycol)s (PEGs) and α-cyclodextrins (α-CDs) have attracted much attention as microtubule biomimicking systems.[26,27] Poly[(ethylene oxide)-*ran*-(propylene oxide)] P(EO-*r*-PO), having a PO content below 20%, also forms inclusion complexes with α-CDs.[28]

[†] National Chiao-Tung University.
[‡] National Synchrotron Radiation Research Center.
* To whom all correspondence should be addressed: e-mail changfc@mail.nctu.edu.tw; Tel 886-3-5727077; Fax 886-3-5719507.

10.1021/ma050254a CCC: $30.25
Published on Web 06/30/2005

In this present system, we introduced α-CDs to poly-[(ethylene oxide)$_{19}$-*ran*-(propylene oxide)$_3$]-*block*-poly(γ-benzyl-L-glutamate) [P(EO_{19}-*r*-PO_3)-*b*-PBLG] diblock copolymers to form α-CD inclusion complexes with the P(EO_{19}-*r*-PO_3) segments; this process led to the preparation of a novel biomaterial, polypseudorotaxane-*block*-PBLG. The formation of these polypseudorotaxanes confines the polymer chain into a rodlike conformation,[29] which changes the original rod−coil chain conformation of the diblock copolymers into a rod−rod conformation. We were interested in exploring how the intrinsic tandem molecular interactions present within and between the blocks (the polypseudorotaxane's channel-type crystallization, the peptide's secondary structure, and microphase separation) can stabilize certain structures and give rise to new materials that possess specific structures and functions. In this paper, we report the preparation of polypeptide-*block*-polypseudorotaxane, and we present a detailed structural investigation of the hierarchical self-assembly of these rod−rod diblock copolymers. We have found that these diblock copolymers display a juxtaposed bilayer-like nanostructure possessing hexagonally packed polypeptide stacks and channel-type polypseudorotaxane moieties.

Experimental Section

Materials. Ethyl acetate (EtOAc) was dried over molecular sieves (4 Å). *N*,*N*′−Dimethylformamide (DMF) was distilled from CaH_2 under reduced pressure and stored over molecular sieves under an argon atmosphere. Primary amine-terminated P(EO_{19}-*r*-PO_3) polymers (JEFFAMINE-brand polyoxyalkyleneamines) were purchased from Huntsman. γ-Benzyl-L-glutamate *N*-carboxyanhydride (Bz-Glu NCA) was prepared according to a literature procedure[30] and stored at −30 °C. α-Cyclodextrin (α-CD) was purchased from Japan TCI Chemical Co. All other solvents and reagents were purchased from commercial suppliers and were used as received.

Synthesis of P(EO_{19}-*r*-PO_3)-*b*-PBLG. A Schlenk flask fitted with a stirrer bar and drying tube was charged with the appropriate amount of Bn-Glu NCA in dry DMF (0.1 g/mL). The required amount of primary amine-terminated P(EO_{19}-*r*-PO_3) was added, and the reaction mixture was stirred at room temperature. After 5 days, the block copolymers were precipitated in diethyl ether, filtered, and vacuum-dried. The precursor P(EO_{19}-*r*-PO_3)-*b*-PBLG was further purified by a Soxhlet extractor before complex with α-CDs. The resultant product was extracted with THF in Soxhlet extractor for 3 days to remove the soluble nonfunctionalized P(EO_{19}-*r*-PO_3) macroinitiator and finally dried at 40 °C in vacuo.

^{1}H NMR (250 MHz, DMSO-d_6): δ = 8.3 (br, 1H × *n*; N*H*), 7.25 (br, 5H × *n*; Bn-*H*), 5.0 (br, 2H × *n*; Bn-CH_2), 4.0 [br, 1H × *n*; (CdO)C*H*RNH], 2.10 (br, 4H × *n*; CH_2CH_2), 0.80 (t, 3H; CH_3). Note: *n* = number-average degree of polymerization of the polypeptide.

Preparation of α-CD Inclusion Complexes. The α-CD·P(EO_{19}-*b*-PO_3)-*block*-PBLG complex (polypseudorotaxane-*block*-polypeptide) assemblies were prepared as follows. A DMF (10 mL) solution containing P(EO_{19}-*r*-PO_3)-*b*-PBLG (0.1 g) was added dropwise to a saturated solution of α-CD (1.45 g) in distilled water (10 mL). The mixture was agitated ultrasonically for 1 h and then left standing for 1 day. The product that precipitated was collected by centrifugation, dried under vacuum, washed with a small portion of distilled water, and then dried again under vacuum to give α-CD-P(EO_{19}-*r*-PO_3)-*b*-PBLG inclusion complexes.

Characterization. The molecular weight and molecular weight distribution were determined by gel permeation chromatography (GPC) using a Waters 510 HPLC−equipped with a 410 differential refractometer, a refractive index (RI) detector, and three Ultrastyragel columns (100, 500, and 10^3 Å) connected in series in order of increasing pore size−using DMF as an eluent at a flow rate of 0.6 mL/min. The molecular weight calibration curve was obtained using poly(ethylene oxide) standards.

^{1}H NMR spectra were recorded in d_6-DMF on a Bruker AM 500 (500 MHz) spectrometer, using the solvent signal as an internal standard.

FT-IR spectra were recorded using a Nicolet Avatar 320 FT-IR spectrometer; 32 scans were collected at a resolution of 1 cm^{-1}. A DMF solution containing the sample was cast onto a NaCl disk and dried under conditions similar to those used in the bulk preparation. The sample chamber was purged with nitrogen to maintain the film's dryness.

High-resolution solid-state ^{13}C NMR spectra were recorded at room temperature using a Bruker DSX-400 spectrometer operating at a resonance frequency of 100.47 MHz. They were acquired using the cross-polarization (CP)/magic angle spinning (MAS)/high-power dipolar decoupling technique.

Thermal analysis through differential scanning calorimetry (DSC) was performed using a DuPont 910 DSC-9000 controller at a scan rate of 10 °C/min over a temperature range from −100 to 160 °C under a nitrogen atmosphere. A small sample (ca. 5−10 mg) was weighed and sealed in an aluminum pan. The sample was quickly cooled to room temperature from the first scan and then scanned between −100 and 160 °C at a scan rate of 10 °C/min. The glass transition temperature was taken as the midpoint of the heat capacity transition between the upper and lower points of deviation from the extrapolated glass and liquid lines.

X-ray diffraction (XRD) measurements were performed using the wiggler beamline BL17A1 of the National Synchrotron Radiation Research Center (NSRRC), Taiwan. Using a triangular bent Si(111) single crystal to obtain a monochromated beam of wavelength λ = 1.3329 Å, XRD patterns were collected using imaging plates (IP; Fuji BAS III, area = 20 × 40 cm^2) curved with a radius equivalent to the sample-to-detector distance (280 mm). With 100 μm pixel resolution of the IP and a typical exposure time of 15 min, the XRD data were measured cover a range of values of Q from 0.2 to 2.2 $Å^{-1}$, where the X-ray vector transfer $Q = 4\pi \sin(\theta/\lambda)$ is defined by the scattering angle 2θ and λ. The two-dimensional powder diffraction patterns observed for the samples (typical diameter 10 mm; thickness 1 mm) were circularly averaged to one-dimensional diffraction profiles $I(Q)$, with Q values calibrated using a standard Si powder.

To cover a wider Q range for a larger scale of structural characteristics and to monitor the correlation of mesoscale and atomic scale orderings of the system during liquid crystal morphological transition, we conducted simultaneous small-angle X-ray scattering (SAXS) and wide-angle X-ray scattering (WAXS) measurements on a dedicated setup at the end-station of the BL01B beamline of the NSRRC. This beamline can deliver a monochromatic beam of ca. 3×10^{11} photons/s at the sample position within the energy range 5−22 keV. Details of the SAXS/WAXS setup were reported recently.[31] We used an X-ray beam of 0.5 mm diameter and a wavelength (λ) of 1.1273 Å for the SAXS/WAXS measurements. With two linear position-sensitive detectors (20 cm in length) located 110 and 30 cm behind the sample position, we collected simultaneously SAXS (with a Q range of 0.015−0.2 $Å^{-1}$) and WAXS profiles (1.0−4.0 $Å^{-1}$). The Q values of the SAXS and WAXS profiles were calibrated using standard samples of polyethylene, Ag behenate, and tripalmitat. The block copolymer samples were sealed between two Kapton windows of 12 μm thickness and measured at 30 °C and an elevated temperature of 100 °C for the phase transition.

Results and Discussion

Preparation and Characterization of Polypeptide-*block*-polypseudorotaxane. Scheme 1 outlines the preparation of the polypeptide-*b*-polypseudorotaxane diblock copolymer. The P(EO_{19}-*r*-PO_3)-*b*-PBLG diblock copolymer was first synthesized through *N*-carboxyanhydride (NCA) polymerization. Primary amine-

Scheme 1. Strategy for the Preparation of the Polypeptide-*block*-polypseudorotaxane

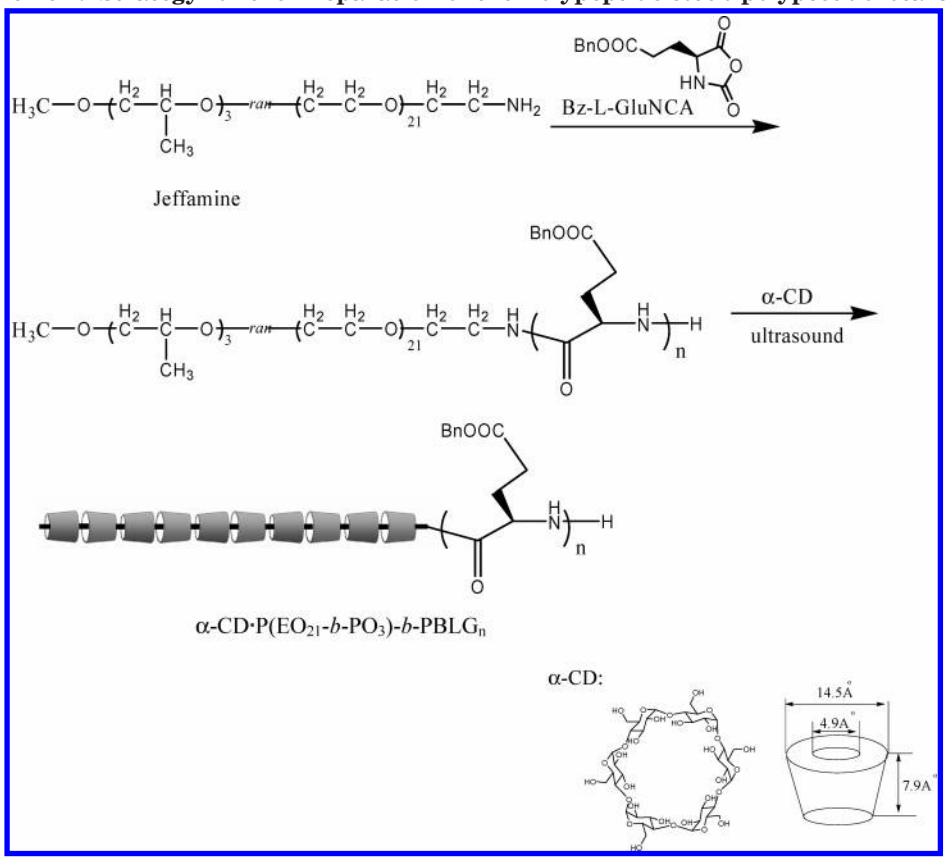

Table 1. Molecular Weight Characteristics of the Block Copolymers

sample	yield (%)[a]	M_n[b]	M_w[b]	M_w/M_n[b]	nGPC[c]	nNMR[d]
$P(EO_{19}$-*r*-$PO_3)$-NH_2		1010	1060	1.05		
$P(EO_{19}$-*r*-$PO_3)$-*b*-$PBLG_{80}$	71	20100	27700	1.38	87	78
$P(EO_{19}$-*r*-$PO_3)$-*b*-$PBLG_{40}$	65	10450	14100	1.35	43	39
$P(EO_{19}$-*r*-$PO_3)$-*b*-$PBLG_{20}$	76	7130	8410	1.18	28	21

[a] Isolated yield, after precipitation and drying. [b] From GPC. GPC experiments were performed using samples dissolved in DMF. [c] Number-average degree of polymerization of the peptide segment, determined by GPC. [d] Number-average degree of polymerization of the peptide segment, determined by ^{1}H NMR spectroscopy (DMSO-d_6).

functionalized $P(EO_{19}$-*r*-$PO_3)$ was used as an initiator for the ring-opening polymerization of γ-benzyl-L-glutamate *N*-carboxyanhydride (Bn-Glu NCA) to afford the desired $P(EO_{19}$-*r*-$PO_3)$-*b*-PBLG diblock copolymer. The diblock copolymers were characterized by ^{1}H NMR spectroscopy and GPC. Table 1 summarizes the molecular characteristics of the block copolymers. The GPC experiments were performed using a refractive index (RI) detector; the system was calibrated using standard poly(ethylene oxide) samples of narrow polydispersity. As a representative example, the GPC trace of the $P(EO_{19}$-*r*-$PO_3)$-*b*-PBLG presented in Figure 1 suggests a polydispersity for the $P(EO_{19}$-*r*-$PO_3)$-*b*-PBLG of ca. 1.2−1.4. Results from GPC and ^{1}H NMR spectroscopy experiments indicate that the length of the polypeptide block depends linearly on the monomer/initiator ratio. This feature is typical of primary amine-initiated polymerizations of α-amino acid *N*-carboxyanhydrides, which, while not living, do provide good control of chain lengths for polypeptides containing up to ca. 100 α-amino acid residues.[32,33]

When a DMF solution of $P(EO_{19}$-*r*-$PO_3)$ was added into an aqueous solution of α-CD, followed by sonication at room temperature, the solution gradually became turbid; ultimately, the inclusion complexes were formed as crystalline precipitates. It has been demonstrated that FTIR spectroscopy, WAXD, and ^{13}C CP/MAS and ^{1}H NMR spectroscopy are useful tools for proving the presence of both the guest and host components in polypseudorotaxanes. Figure 2 presents the FTIR spec-

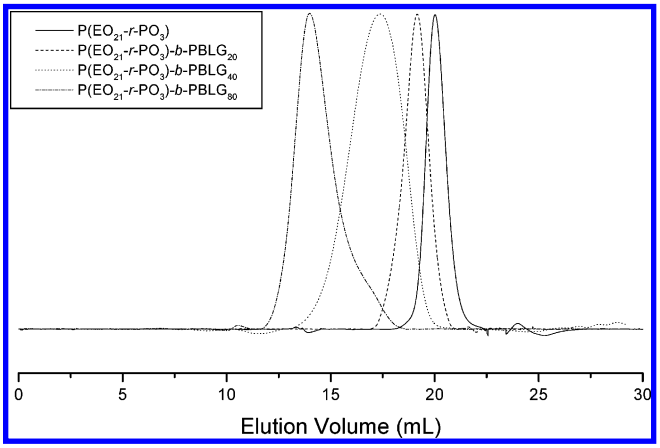

Figure 1. GPC traces (refractive index detector signal) of the primary amine-terminated $P(EO_{19}$-*b*-$PO_3)$ macroinitiator and the $P(EO_{19}$-*b*-$PO_3)$-*b*-PBLG block copolymers.

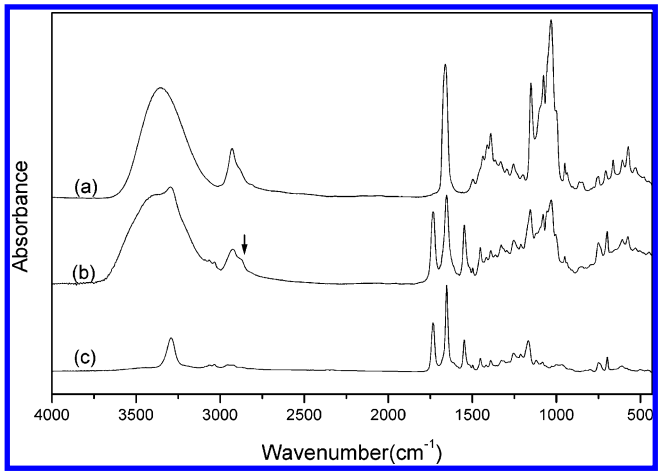

Figure 2. FTIR spectra of (a) α-CD, (b) the α-CD·P(EO_{19}-*b*-PO_3)-*b*-PBLG complex, and (c) P(EO_{19}-*b*-PO_3)-*b*-PBLG.

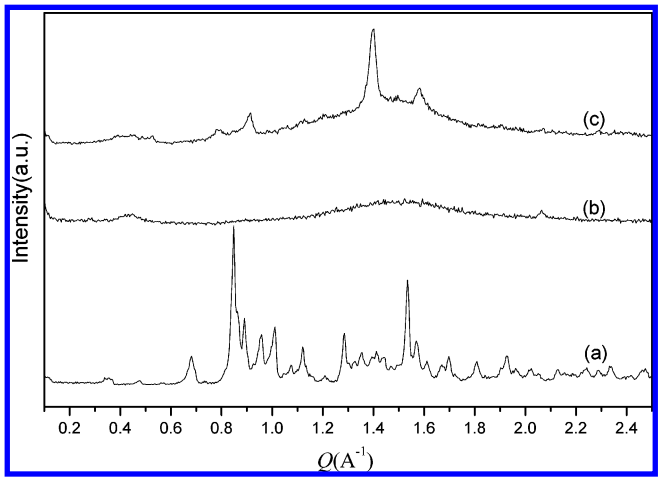

Figure 3. XRD diffraction patterns recorded at room temperature for (a) α-CD, (b) P(EO_{19}-*r*-PO_3)-*b*-$PBLG_{20}$, and (c) the α-CD·P(EO_{19}-*r*-PO_3)-*b*-$PBLG_{20}$ complex.

tra of pure α-CD, the α-CD·P(EO_{19}-*r*-PO_3)-*b*-PBLG complex, and P(EO_{19}-*r*-PO_3)-*b*-PBLG recorded over the region from 400 to 4000 cm^{-1}. The signal of the O−H stretching mode at 3350 cm^{-1} of the α-CD shifts to 3360 cm^{-1} as upon forming the α-CD·P(EO_{19}-*r*-PO_3)-*b*-PBLG inclusion complex. The decrease in the intensity of the broad band at 3300 cm^{-1} (O−H stretching) relative to that at 2930 cm^{-1} (C−H stretching) and the new band generated as a shoulder at 2877 cm^{-1} (C−H stretching) also provide additional evidence for inclusion complex formation.[34] The distinctive bands at 1730 cm^{-1} (C═O stretching) and 1545 cm^{-1} (N−H bending) in the α-CD·P(EO_{19}-*r*-PO_3)-*b*-PBLG complex (Figure 2b) reveals features of the PBLG blocks after the formation of the inclusion complex.

Figure 3 presents a comparison of the XRD patterns observed for α-CD, P(EO_{19}-*r*-PO_3)-*b*-PBLG, and the α-CD·P(EO_{19}-*r*-PO_3)-*b*-PBLG complex at room temperature. Major XRD peaks for pure α-CD are observed at $Q = 0.680$, 0.850, 1.292, and 1.515 $Å^{-1}$, whereas P(EO_{19}-*r*-PO_3)-*b*-PBLG displays only a broad, amorphous, diffuse peak. There are significantly fewer crystalline peaks for the inclusion complex α-CD·P(EO_{19}-*r*-PO_3)-*b*-PBLG relative to those of pure α-CD. Nevertheless, the strong reflection at $Q \approx 1.38$ $Å^{-1}$ indicates that in the crystalline inclusion complexes the α-CD molecules are stacked along the P(EO_{19}-*r*-PO_3) axis to form channel-type structures.[20,21,28]

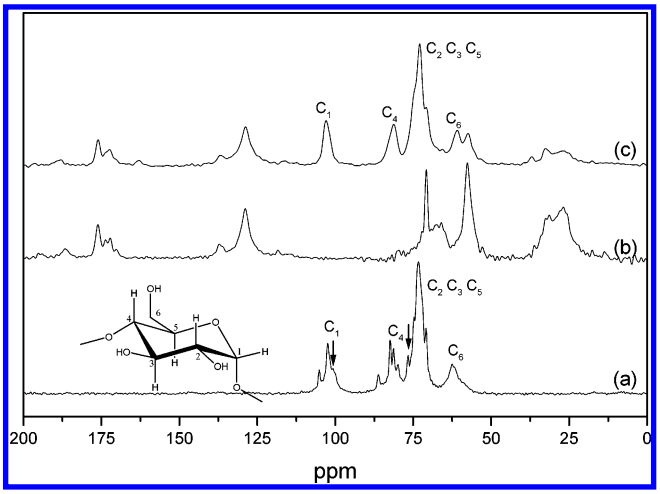

Figure 4. Solid-state ^{13}C CP/MAS NMR spectra of (a) α-CD, (b) P(EO_{19}-*r*-PO_3)-*b*-$PBLG_{20}$, and (c) the α-CD·P(EO_{19}-*r*-PO_3)-*b*-$PBLG_{20}$ complex.

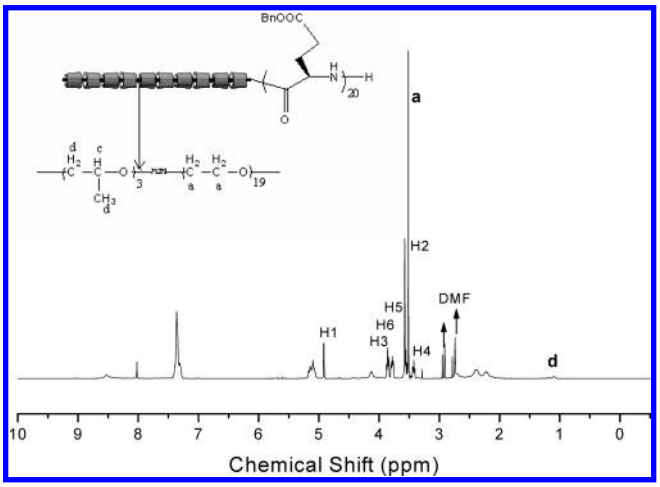

Figure 5. 500 MHz ^1H NMR spectra of the α-CD·P(EO_{19}-*r*-PO_3)-*b*-$PBLG_{20}$ complex recorded in DMF-d_6.

Solid-state ^{13}C CP/MAS NMR spectroscopy studies can provide additional information about the structure of α-CD complexes. Figure 4a displays the spectrum of α-CD, which is known to assume a less symmetrical conformation in its crystalline uncomplexed state. In this case, the spectrum reveals resolved C1 and C4 resonances; i.e., these atoms are located adjacent to a single conformationally strained glycosidic linkage. In contrast, these resolved resonances disappear in Figure 4c for the α-CD·P(EO_{19}-*r*-PO_3)-*b*-PBLG complex, in which each carbon atom of the glucose unit of the α-CD experiences a similar environment.

The stoichiometry of the polypseudorotaxane can be determined by ^1H NMR spectroscopy. Figure 5 displays the ^1H NMR spectrum of the α-CD·P(EO_{19}-*r*-PO_3)-*b*-$PBLG_{20}$ complex in DMF-d_6. A comparison between the intensities of the integral of the peaks for α-CD and those for the P(EO_{19}-*r*-PO_3) blocks provides the composition of the polypseudorotaxane: we obtained the ratio of α-CD units to these blocks to be ca. 10 for the α-CD·P(EO_{19}-*r*-PO_3)-*b*-$PBLG_{20}$ complex. Considering the composition of the copolymer, the molar ratio of EO units to α-CD moieties is 2:1 for this polypseudorotaxane, which matches perfectly the stoichiometry reported previously for the α-CD·PEO complex.[21] This result indicates that, in the α-CD·P(EO-*r*-PO) polypseudorotaxanes, only the EO segments are encircled by α-CD

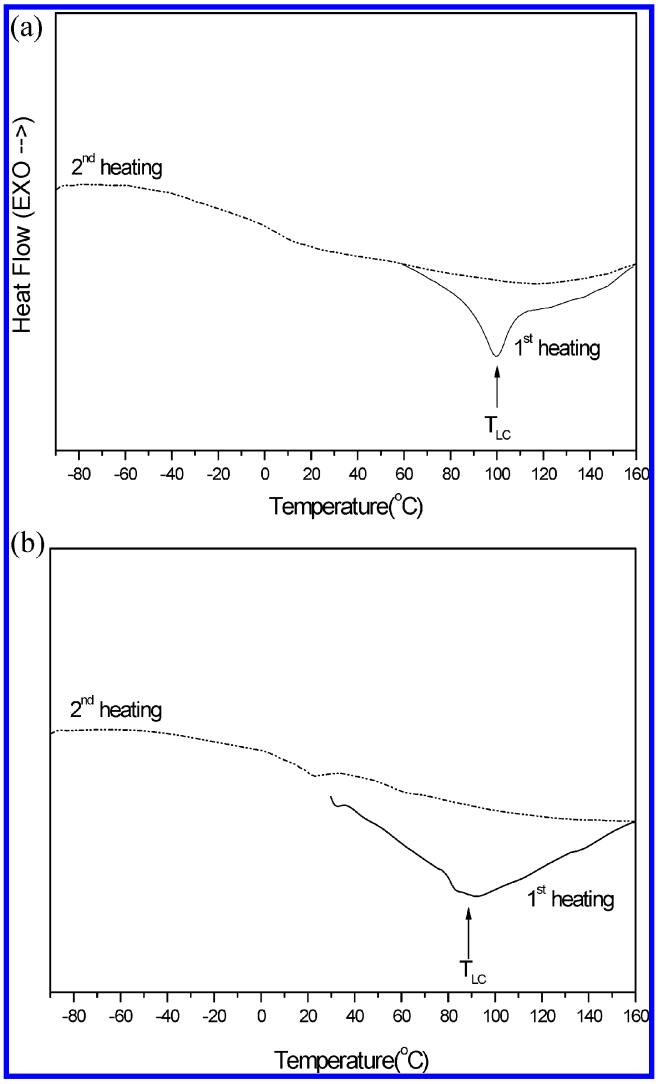

Figure 6. DSC thermograms of (a) P(EO_{19}-*r*-PO_3)-*b*-$PBLG_{20}$ and (b) the α-CD·P(EO_{19}-*r*-PO_3)-*b*-$PBLG_{20}$ complex.

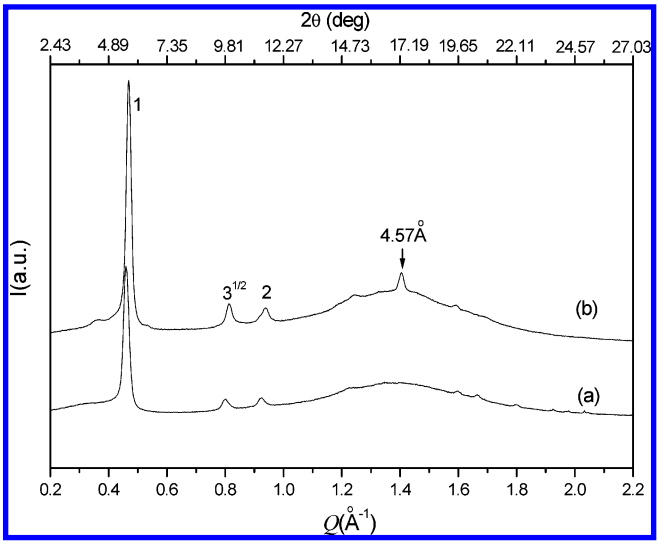

Figure 7. XRD data for (a) P(EO_{19}-*r*-PO_3)-*b*-$PBLG_{80}$ and (b) the α-CD·P(EO_{19}-*r*-PO_3)-*b*-$PBLG_{80}$ complex, both recorded at 120 °C.

units; the PO units distributed randomly within the copolymer chain remain mostly uncovered. Although the dimensions of a PO unit are not ideal for forming a particularly stable inclusion complex with α-CD, there is no significant steric or energy barrier that restricts the motion of the CD toroid as it passes around PO units or short PO segments. Consequently, the P(EO_{19}-*r*-PO_3) chain can penetrate the α-CD cavity freely such that stable inclusion complex "segments" are formed between the α-CD moieties and the EO units of P(EO_{19}-*r*-PO_3)-*b*-$PBLG_{20}$.

Supramolecular Organization in the Bulk State. We performed DSC, WAXS, and SAXS experiments to elucidate the supramolecular organization of the polypeptide-*block*-polypseudorotaxane diblock copolymers; the CD units of the polypseudorotaxanes loop tightly around the flexible P(EO_{19}-*r*-PO_3) chains, causing them to reorganize into stiff rods. The DSC data reveal specific transitions of these block copolymers, as shown in the representative DSC traces (Figure 6a,b) for the P(EO_{19}-*r*-PO_3)-*b*-$PBLG_{20}$ and its inclusion complex α-CD·P(EO_{19}-*r*-PO_3)-*b*-$PBLG_{20}$, respectively. In the DSC curve observed for the system without α-CD inclusion (Figure 6a), the features of the P(EO_{19}-*r*-PO_3) block are absent because of the short PEO chain length of little crystallization (as also evidenced from the corresponding WAXS data shown below), whereas the phase transition of the PBLG block can be identified by a endothermic peak displaying a typically low enthalpic change at ca. 100 °C (T_{LC}, a nematic-like paracrystalline phase). The observed transition is irreversible and occurs only during the first heating run. We attribute this result to the irreversible change of the peptide from a 7/2 to an 18/5 α-helical conformation.[15,35] The α-helix, stabilized by intramolecular hydrogen bonds of its residues along the helix, possesses a helix pitch of ca. 5.4 Å. The helix, which involves ca. 3.6 residues per turn or 18 residues in five turns, is right-handed for L-α-amino acids. On the other hand, the PBLG phase transition endothermic peak around ~100 °C is broadened significantly in the DSC curve (Figure 6b) observed for the complex system with the inclusion of α-CD, implying a complicated phase transition behavior that involves at least three types of interactions, namely PBLG liquid crystallization, the polypseudorotaxane's channel-type crystallization, and microphase separation between the peptide and the polypseudorotaxane. The competition between these forces for a self-assembly structure of a minimized free energy of the system is further investigated by WAXS and simultaneously SAXS/WAXS measurements for monitoring the simultaneously changes of the crystallization and microphase separation in the system, as detailed below.

In an effort to further characterize the structures of these rod−rod diblock copolymers, XRD measurement were performed to elucidate self-assembly structure of the polypeptide-*block*-polypseudorotaxane. In Figures 7−9, we present the WAXS data measured at 120 °C, i.e., above the phase transition temperature, for the peptide-based diblock copolymers at three different polymer−peptide ratios: P(EO_{19}-*r*-PO_3)-*b*-$PBLG_{80}$, P(EO_{19}-*r*-PO_3)-*b*-$PBLG_{40}$, and P(EO_{19}-*r*-PO_3)-*b*-$PBLG_{20}$, before and after formation of their inclusion complexes with α-CD. According to the DSC results discussed above, the PBLG blocks possess a liquid-crystalline phase. Correspondingly, XRD data for all of the samples display a set of Bragg peaks at $Q = 0.45$, 0.78, and 0.90 $Å^{-1}$ in a ratio of $1:3^{1/2}:2$. This ratio corresponds to a columnar hexagonal organization of the polypeptide α-helix in the liquid-crystalline phase. The lattice

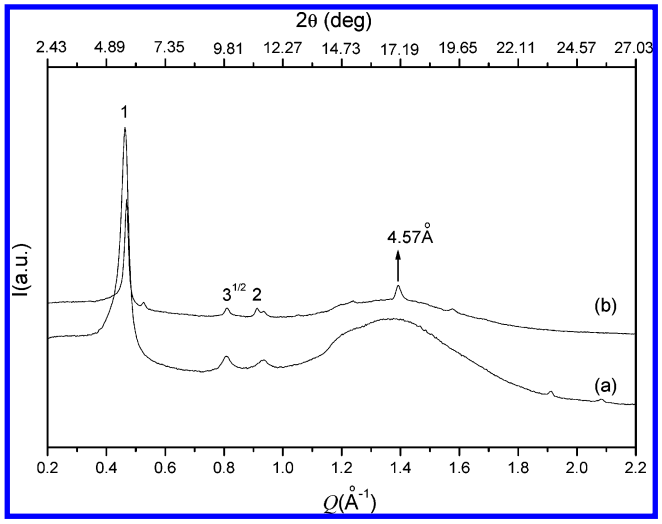

Figure 8. XRD data for (a) P(EO_{19}-*r*-PO_3)-*b*-$PBLG_{40}$ and (b) α-CD·P(EO_{19}-*r*-PO_3)-*b*-$PBLG_{40}$ complex, both recorded at 120 °C.

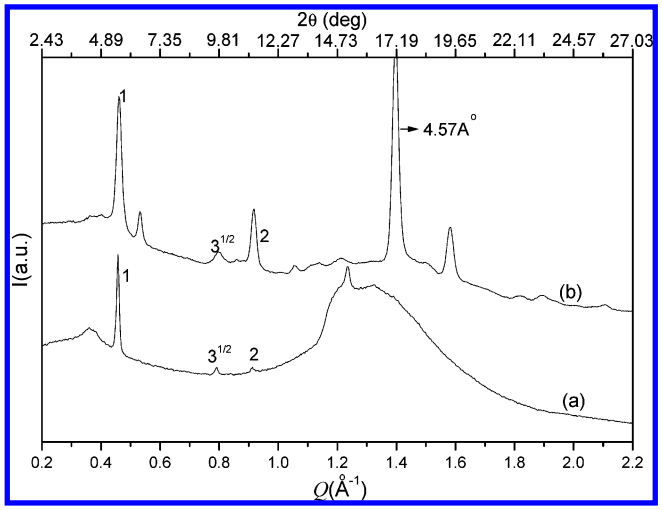

Figure 9. XRD data for (a) P(EO_{19}-*r*-PO_3)-*b*-$PBLG_{20}$ and (b) α-CD·P(EO_{19}-*r*-PO_3)-*b*-$PBLG_{20}$ complex, both recorded at 120 °C.

parameter, ca. ~14 Å, of the hexagonal structure extracted from the scattering peak positions fits well to the intermolecular distance between neighboring poly(γ-benzyl-L-glutamate) chains.[14,15] In contrast, the two nonnegligible peaks at $Q \sim 0.32$ and 1.3 $Å^{-1}$ appeared in Figure 9a, implying that the coil−rod P(EO_{19}-*r*-PO_3)-*b*-$PBLG_{20}$ (before α-CD inclusion) also exhibits the lamellar structural characteristics of β-sheet polypeptides, in additional to the hexagonal array of α-helical peptides, in the system after the phase transition, as also observed in a similar system by Lecommandoux et al.[15] Interestingly, the β-sheet structure is suppressed significantly in the rod−rod system of α-CD·P(EO_{19}-*r*-PO_3)-*b*-$PBLG_{20}$ (see the greatly diminished peaks at $Q \sim 0.32$ and 1.23 $Å^{-1}$ in Figure 9b), due presumably to the weakening of intermolecular hydrogen bonding after channel-type crystalline formation which disfavor β-sheet conformation of the peptides. In addition, we could also approximately evaluate the low β-sheet content in α-CD·P(EO_{19}-*r*-PO_3)-*b*-$PBLG_{20}$ from the trivial β-sheet amide I band at 1630 cm^{-1} in FTIR spectra (Figure 2b) and 52.36 ppm β-sheet amide C=O resonance in ^{13}C solid-state NMR (Figure 4c).[14,15,19] Furthermore, we observed (Figures 7b, 8b, and 9b) a strong characteristic Bragg peak at $Q = 1.38$ $Å^{-1}$ (d = 4.57 Å) for each of the three copolymer inclusion complexes with α-CD. The Bragg peak $q = 1.38$ $Å^{-1}$ was regarded as a signature peak for the channel-type crystalline structure of polypseudorotaxane of α-CDs after threaded in the P(EO_{19}-*r*-PO_3), as reported by Harada et al. and Li et al.[20,21,28]

Upon a closure look at the XRD data, we found that the set of the scattering peaks for the peptide hexagonal packing of the P(EO_{19}-*r*-PO_3)-*b*-polypeptide after α-CD inclusion had shifted slightly from those in the absence of α-CD, especially for the α-CD·P(EO_{19}-*r*-PO_3)-*b*-$PBLG_{80}$ complex, which contains the richest relative abundance of peptides. This observation may be a consequence of the crystalline competition between the peptides and the copolymer upon α-CD inclusion. In any case, these WAXS data indicate that the block copolymers are phase-separated into domains presenting a columnar hexagonal arrangement of α-helical polypeptide and polypseudorotaxanes in channel-type crystallization. These two crystalline structures, namely, linear channel-type and planar hexagonal packing, which possess different degrees of freedom, coexist in the system. In addition, among the three block copolymers, the WAXS pattern of the α-CD·P(EO_{19}-*r*-PO_3)-*block*-$PBLG_{20}$ complex displays the highest crystallinity (the amorphous type peak is absent in the pattern) in the bulk state. Presumably, the α-CD·P(EO_{19}-*r*-PO_3)-*block*-$PBLG_{20}$ complex, having an optimized ratio of polypeptides blocks and polypseudorotaxanes, can accommodate better the coexisting orderings of both blocks.

Gallot et al.[37−41] have used SAXS to investigate the solid-state morphologies of linear polyvinyl−polypeptide coil−rod block copolymers. They found a large-scale hexagonal-in-lamellar morphology of the alternating polyvinyl and polypeptide sheets with the α-helical polypeptide chains arranged in a hexagonal array. To observe the correlation between the self-assembly of the hexagonally packed polypeptide and the channel-type crystallization of the polypseudorotaxane, we have conducted simultaneous SAXS/WAXS measurements for the α-CD·P(EO_{19}-*r*-PO_3)-*b*-$PBLG_{20}$ complex, of the highest channel-type crystallinity of α-CD among the three complexes studied. Figure 10a presents the simultaneous changes in the WAXS and SAXS profiles when the sample temperature was increased from room temperature to 100 °C (the phase transition temperature T_{LC}). In the inset of Figure 10a, the Bragg peak $Q \approx 1.38$ $Å^{-1}$ for the channel-type crystalline phase (WAXS data) grows at T_{LC}, with concomitant formation of a broad bump at $Q = 0.025$ $Å^{-1}$ in the SAXS profile. The broad peak, assumed to be a Bragg reflection, corresponds to an ordering spacing of 250 Å. Structurally speaking, the PBLG repels α-CD units from its crystalline domains; meanwhile, the scattered α-CDs gather and lock into the copolymers to form channel-type crystalline entities. The cleaner system can now phase separate into two different types of crystalline domains, which further pack into a lamellar-like sequence having a bilayer structure. The characteristic spacing (250 Å) observed from the SAXS data is correlated to the bilayer structure of the α-CD·P(EO_{19}-*r*-PO_3)-$PBLG_{20}$ complex (Scheme 2). The observed spacing is close to the thickness (233 Å) expected for the repeated packing of the "{α-CD·P(EO_{19}-*r*-PO_3) rods}-{$PBLG_{20}$ α-helical rods}-{$PBLG_{20}$ α-helical rods}-{α-CD·P(EO_{19}-*r*-PO_3) rods}" bilayer structure, which we esti-

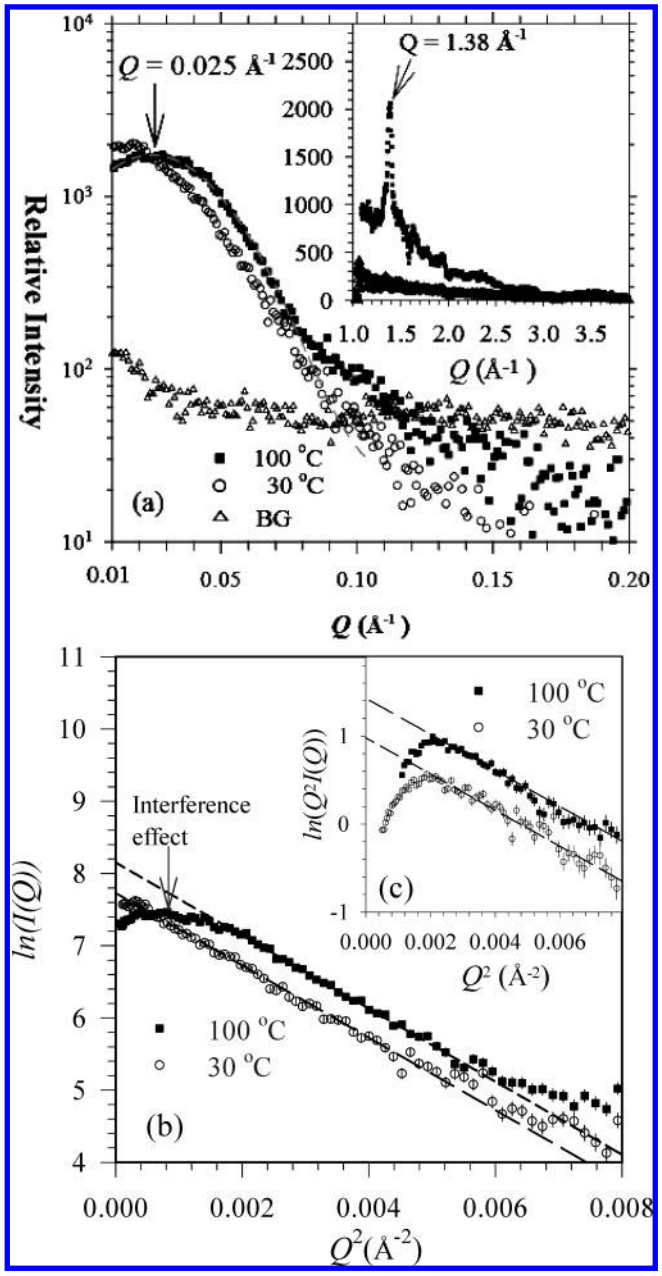

Figure 10. (a) Simultaneous SAXS and WAXS (inset) data, with the background (BG) scattering (△) subtracted, for the α-CD·P(EO_{19}-*r*-PO_3) -*b*-$PBLG_{20}$ complex at 30 and 100 °C. The broad bump in the SAXS data is fitted (dashed curve) by a Gaussian profile peaked at 0.025 $Å^{-1}$. (b) SAXS data for the complex α-CD·P(EO_{19}-*r*-PO_3)-*b*-$PBLG_{20}$ are represented in a Guinier plot for elucidating the interference effect induced by temperature (dashed lines are Guinier approximations for the respective data). (c) SAXS data for the complex α-CD·P(EO_{19}-*r*-PO_3)-*b*-$PBLG_{20}$ are represented in a Kratky−Porod plot for elucidating the slablike structural characteristics of the sample (dashed lines are Kratky−Porod approximations for extracting the slablike thickness).

mated from the twice the sum of the copolymer length (3.6 Å × 24) and peptide length (20/3.6 × 5.4 Å). For this calculation, we estimated the length of the polypseudorotaxane by considering the length of a fully stretched P(EO_{19}-*r*-PO_3) unit (3.6 Å is the maximum extension of each EO or PO unit), which allows 10 α-CD units to be accommodated (consistent with the NMR result); we estimated the length of the polypeptide segment by considering the 18/5 α-helical conformations to have a 5.4 Å length for each pitch of the helix.

Scheme 2. Proposed Model for the Self-Assembly of the Polypeptide-*block*-polypseudorotaxane at a Temperature Larger Than the Value of T_{LC} of PBLG

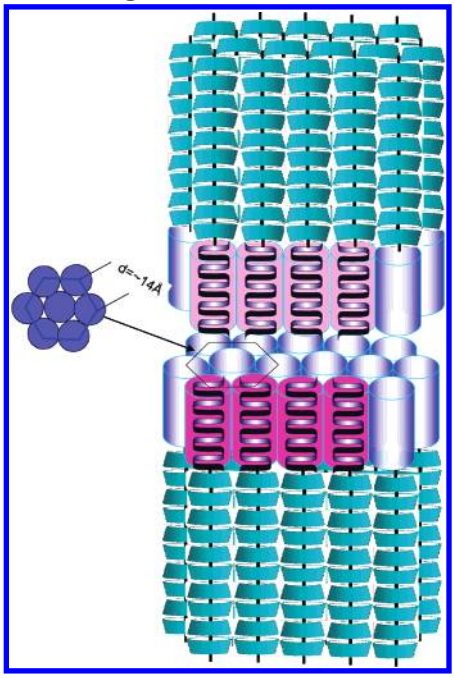

Estimated from the peak width of the SAXS interference peak, the ordering range is ∼50 nm, corresponding to a few bilayer stacking. Likely, domains of an in-plane hexagonal packing and an across-plane stacking, in a space of ∼ 40 × 40 × 50 nm^3 (estimated from the interference peak widths of the XRD and SAXS data), may represent the sample structure above 100 °C better. In Figure 10b, the SAXS data are represented in a Guinier plot in the low-*Q* region (Q^2 < 0.002 $Å^{-2}$) for elucidating the interference effect induced by temperature.[36] The SAXS data measured at 30 °C can be fitted well using the Guinier approximation (long dashed line), indicating that the scattering is mainly dominated by the form factor of the scattering objects. On the other hand, the SAXS data measured at 100 °C significantly deviate from the Guinier approximation (short dashed line) in the low-*Q* region, indicating the existence of an interference effect between the aggregates. In Figure 10c, SAXS data for the complex α-CD·P(EO_{19}-*r*-PO_3)-*b*-$PBLG_{20}$ are represented in a Kratky−Porod plot[36] for elucidating the slablike structural characteristics of the sample. Both sets of data can be fitted using the Kratky−Porod approximation (dashed lines) in the intermediate-*Q* region, and a common thickness $t = 5 \pm 0.5$ nm for the slabs is extracted from the slope *m* of the dashed lines, using $m^2 = t^2/12$.[36] This analysis implies that a slablike structure formed at 30 °C, and the slablike structure persists at 100 °C. The thickness 5 nm obtained is close to a bilayer packing of peptides of the molecules, in the direction perpendicular to the hexagonal packing plane. At 100 °C, the block copolymer part also forms a hexagonal packing corresponding to the peptide part (from the XRD data), which enhances the ordering of the bilayer stacking in the system.

The SAXS analysis suggests that the arrangement of the polypeptide helices of this rod−rod diblock copolymer is in a "stacking" mode, which differs from the interdigitation or folding arrangement of the polyvinyl-*b*-polypeptide coil−rod system.[37−40] The stacking arrangement of the helices can be explained by a favorable

close-packing of the polypseudorotaxane. The stacking arrangement can also be revealed from the geometrical factor $\gamma = (8 \times 10^{21}/\pi N_A)(M_n/\rho d d_H^2)$ obtained by dividing the molecular volume by the average lateral extension of a chain ($d/2$; interface area per chain) and the cross section of a helix ($d_H^2\pi/4$),[41] where l_H is the maximum length of a poly(γ-benzyl-L-glutamate) α-helix, d_H the spacing between helices, and d the intersheet spacing.[41] As illustrated in Scheme 2, stacked helices give $\gamma = 1$, whereas interdigitated or folded helices reveal two unit areas per chain or $\gamma = 2$. We observed that the value of γ for the α-CD·P(EO_{19}-*r*-PO_3)-*b*-$PBLG_{20}$ complex is 0.8, which is close to 1, using $l_H = 3$ nm, $d_H = 1.35$ nm, $d = 23.3$ nm, and $\rho = 1.001$ g/mL. This value indicates that the helices of this rod−rod block copolymer prefer "stacked" rather than interdigitated or folded.

According to the discussion above, we conclude that the competing and cooperating interactions within and between polypeptide-*block*-polypseudorotaxane units—including PBLG liquid crystallization, the polypseudorotaxane's channel-type crystallization, microphase separation, and entropy—lead to a minimization of the free energy of the system that results in the hierarchical structures observed. However, in view of the complicated crystallization forces coexisting in the system, phase separation or self-assembled morphology of the system with different chain lengths of either the polypeptide or polypseudorotaxane block, leading to different crystallization strengths, will be difficult to be envisaged without a systematic study.

Conclusions

In this paper, we have described the preparation and supramolecular organization of a novel biomaterial: a polypeptide-*block*-polypseudorotaxane. These diblock copolymers comprise α-helical polypeptide rods based on γ-benzyl-L-glutamate (PBLG) on one end and coil-segmented P(EO_{19}-*r*-PO_3) that thread through α-cyclodextrin (α-CD) units to form inclusion complexes (polypseudorotaxanes) on the other. The P(EO_{19}-*r*-PO_3)-*b*-PBLG diblock copolymers were synthesized by *N*-carboxyanhydride (NCA) polymerization using primary amine-functionalized P(EO_{19}-*r*-PO_3) as macroinitiators; we have characterized the resulting block copolymers by GPC and ^{1}H NMR spectroscopy. The formation of channel-type structures for the polypseudorotaxanes is clearly and consistently evidenced by a series of FTIR, ^{13}C CP/MAS NMR, and ^{1}H NMR spectroscopic and WAXS measurements.

For the self-assembled structure, the DSC, XRD, and simultaneous SAXS/WAXS data suggest that the block copolymers are phase-separated into domains containing a liquid-crystalline columnar hexagonal arrangement of α-helical PBLG units stacked with channel-type crystallization of the polypseudorotaxanes. Furthermore, these two ordered domains form a hierarchical structure possessing bilayer characteristics. Competition and cooperation among PBLG liquid crystallization, the polypseudorotaxane's channel-type crystallization, microphase separation of the peptide and copolymers, and entropy lead to minimization of the free energy of the system that results in the hierarchical structures observed for the α-CD·P(EO_{19}-*r*-PO_3)-*b*-$PBLG_{20}$ complex, namely, bilayer-like nanostructure possessing planar hexagonally packed PBLG and a channel-type polypseudorotaxane.

Acknowledgment. The authors thank Drs. M. H. J. Koch, A. Gabriel, Y.-S. Sun, and Y.-H. Lai for the help in the simultaneous SAXS/WAXS measurement.

References and Notes

(1) Muthukumar, M.; Ober, C. K.; Thomas, E. L. *Science* **1997**, *277*, 1225.
(2) Stupp, S. I.; Braun, P. V. *Science* **1997**, *277*, 1242.
(3) Lee, M.; Cho, B.-K.; Zin, W. C. *Chem. Rev.* **2001**, *101*, 3869.
(4) Klok, H. A.; Lecommandoux, S. *Adv. Mater.* **2001**, *13*, 1217.
(5) Kong, X.; Jenekhe, S. A. *Macromolecules* **2004**, *37*, 8180.
(6) McMillan, A.; Lee, T. A. T.; Conticello, V. P. *Macromolecules* **1999**, *32*, 3643.
(7) Halstenberg, S.; Panitch, A.; Rizzi, S.; Hall, H.; Hubbell, J. A. *Biomacromolecules* **2002**, *3*, 710.
(8) Gehrke, S. H. *Adv. Polym. Sci.* **1993**, *110*, 81.
(9) Lee, K. Y.; Mooney, D. J. *Chem. Rev.* **2001**, *101*, 1869.
(10) Kaplan, D. L. *Polym. Degrad. Stab.* **1998**, *59*, 25−32.
(11) Chen, J. T.; Thomas, E. L.; Ober, C. K.; Mao, G. P. *Science* **1996**, *273*, 343.
(12) Gallot, B. *Prog. Polym. Sci.* **1996**, *21*, 1035.
(13) Cornelissen, J. J. L. M.; Fischer, M.; Sommerdijk, N. A. J. M.; Nolte, R. J. M. *Science* **1998**, *280*, 1427.
(14) Klok, H. A.; Langenwalter, J. F.; Lecommandoux, S. *Macromolecules* **2000**, *33*, 7819.
(15) Lecommandoux, S.; Achard, M. F.; Langenwalter, J. F.; Klok, H. A. *Macromolecules* **2001**, *34*, 9100.
(16) Schlaad, H.; Kukula, H.; Smarsly, B.; Antonietti, M.; Pakula, T. *Polymer* **2002**, *43*, 5321.
(17) Caillol, S.; Lecommandoux, S.; oise Mingotaud, A. F.; Schappacher, M.; Bryson, A. S. N.; Meyrueix, R. *Macromolecules* **2003**, *36*, 1118.
(18) Block, H. In *Poly(γ-benzyl-L-glutamate) and Other Glutamic Acid Containing Polymers*; Gordon and Breach Science Publishers: New York, 1983.
(19) Papadopoulos, P.; Floudas, G.; Klok, H.-A.; Schnell, I.; Pakula, T. *Biomacromolecules* **2004**, *5*, 81.
(20) Harada, A.; Kamachi, M. *Macromolecules* **1990**, *23*, 2821.
(21) Harada, A.; Lin, J.; Kamachi, M. *Macromolecules* **1993**, *26*, 5698.
(22) Harada, A.; Nishiyama, T.; Kawaguchi, Y.; Okada, M.; Kamachi, M. *Macromolecules* **1997**, *30*, 7115.
(23) Kawaguchi, Y.; Nishiyama, T.; Okada, M.; Kamachi, M.; Harada, A. *Macromolecules* **2000**, *33*, 4472.
(24) Rusa, C. C.; Luca, C.; Tonelli, A. E. *Macromolecules* **2001**, *34*, 1318.
(25) Li, J.; Ni, X.; Zhou, Z.; Leong, K. W. *J. Am. Chem. Soc.*. **2003**, *125*, 1788.
(26) Harada, A.; Li, J.; Kamachi, M. *Nature (London)* **1992**, *356*, 325−327; **1993**, *364*, 516; **1994**, *370*, 126.
(27) Hwang, M. J.; Bae, H. S.; Kim, S. J.; Jeong, B. *Macromolecules* **2004**, *37*, 8820.
(28) Li, J.; Li, X.; Toh, K. C.; Ni, X.; Zhou, Z.; Leong, K. W. *Macromolecules* **2003**, *37*, 8820.
(29) Shimomura, T.; Yoshida, K. I.; Ito, K.; Hayakawa, R. *Polym. Adv. Technol.* **2001**, *11*, 837.
(30) Daly, W. H.; Poche, D. *Tetrahedron Lett.* **1988**, *29*, 5859.
(31) Lai, Y. H.; Sun, Y. S.; Jeng, U.; Huang, Y.-S.; Song, Y. F.; Tsang, K. L.; Liang, K. S. *Nucl. Instrum. Methods Phys. Res. B*, in press.
(32) Deming, T. J. *Adv. Mater.* **1997**, *9*, 299.
(33) Deming, T. J. *J. Polym. Sci., Part A: Polym. Chem.* **2000**, *38*, 2011.
(34) Huang, L.; Allen, E.; Tonelli, A. E. *Polymer* **1998**, *39*, 4857.
(35) Watanabe, J.; Uematsu, I. *Polymer* **1984**, *25*, 1711.
(36) Glatter, O.; Kratky, O. *Small Angle X-ray Scattering*; Academic Press: London, 1980.
(37) Billot, J. P.; Douy, A.; Gallot, B. *Makromol. Chem.* **1976**, *177*, 1889.
(38) Perly, B.; Douy, A.; Gallot, B. *Makromol. Chem.* **1976**, *177*, 2569.
(39) Billot, J. P.; Douy, A.; Gallot, B. *Makromol. Chem.* **1977**, *178*, 641.
(40) Douy, A.; Gallot, B. *Polymer* **1982**, *23*, 1039.
(41) Schlaad, H.; Kukula, H.; Smarsly, B.; Antonietti, M.; Pakula, T. *Polymer* **2002**, *43*, 5321.

MA050254A